University of Massachusetts Amherst
ScholarWorks@UMass Amherst

Masters Theses | Dissertations and Theses

October 2021

Spatiotemporal Metabolic Modeling of Pseudomonas aeruginosa Biofilm Expansion

Robert Sourk
University of Massachusetts at Amherst

Follow this and additional works at: https://scholarworks.umass.edu/masters_theses_2

 Part of the Biochemical and Biomolecular Engineering Commons, and the Transport Phenomena Commons

Recommended Citation

Sourk, Robert, "Spatiotemporal Metabolic Modeling of Pseudomonas aeruginosa Biofilm Expansion" (2021). *Masters Theses*. 1135.
https://doi.org/10.7275/24889430.0 https://scholarworks.umass.edu/masters_theses_2/1135

This Open Access Thesis is brought to you for free and open access by the Dissertations and Theses at ScholarWorks@UMass Amherst. It has been accepted for inclusion in Masters Theses by an authorized administrator of ScholarWorks@UMass Amherst. For more information, please contact scholarworks@library.umass.edu.

Spatiotemporal Metabolic Modeling of *Pseudomonas aeruginosa* Biofilm Expansion

A Thesis Presented

By

ROBERT L. SOURK II

Submitted to the Graduate School of the

University of Massachusetts Amherst in partial fulfilment

of the requirements for the degree of

MASTER OF SCIENCE IN CHEMICAL ENGINEERING

September 2021

Department of Chemical Engineering

Spatiotemporal Metabolic Modeling of *Pseudomonas aeruginosa* Biofilm Expansion

A THESIS PRESENTED

By

ROBERT L. SOURK II

Approved by:

_____

Michael Henson, Chair

_____

Jessica Schiffman, Member

_____

Dr. Michael Henson, Department Head
Chemical Engineering

EPIGRAPH

"Anyone can achieve their fullest potential, who we are might be predetermined, but the path we follow is always of our own choosing. We should never allow our fears or the expectations of others to set the frontiers of our destiny. Your destiny cannot be changed but, it can be challenged. Every individual is born as many individuals and dies as one."

— Martin Heidegger

*Note: This quote was adapted to be inclusive to all genders.

ACKNOWLEDGMENTS

I would like to give Dr. Michael Henson due credit for taking me on as student and allowing me to work on this project. Dr. Henson has also guided me throughout this whole process and his knowledge of numerical simulations and biofilms was key for me to complete this thesis. Furthermore, the Henson Research Group helped me gain a in depth idea of the key numerical idea that govern my research. Specifically, Ayushi Patel helped me understand Flux Balance Analysis. Dr. Poonam Phalak gave me access to the SFBA code that I altered to simulate the results.

ABSTRACT

SPATIOTEMPORAL METABOLIC MODELING OF PSEUDOMONAS AERUGINOSA BIOFILM EXPANSION

SEPTEMBER 2021

ROBERT L. SOURK II, B.S. IOWA STATE UNIVERSITY

MSCHE, UNIVERSITY OF MASSACHUSETTS AMHERST

Directed by Michael Henson

Spatiotemporal metabolic modeling of microbial metabolism is a step closer to achieving higher dimensionalities in numerical studies (*in silico*) of biofilm maturation. Dynamic Flux Balance Analysis (DFBA) is an advanced modeling technique because this method incorporates Genome Scale Metabolic Modeling (GSMM) to compute the biomass growth rate and metabolite fluxes. Biofilm thickness is pertinent because this variable of biofilm maturation can be measured in a laboratory (*in vitro*). *Pseudomonas aeruginosa* (*P. aeruginosa*) is the model bacterium used in this computational model based on previous research conducted by Dr. Michael Henson, available GSMMs, and the societal significance of patients suffering from *P. aeruginosa* airway infections. Spatiotemporal Flux Balance Analysis (SFBA) will be the computational method used in this thesis to simulate biofilm growth. Another level of accuracy will be introduced to SFBA which is a dynamic finite difference grid that will vary relative to the biofilm's velocity of expansion/contraction. This novel idea is governed by a differential equation that defines the biofilm's velocity and updates the spatial dependency of the finite difference grid which has never been done while utilizing GSMM. Environmental conditions (bulk concentrations of metabolites) are altered to investigate how varying nutrients (glucose, oxygen, lactate, nitrate) affected biofilm maturation.

TABLE OF CONTENTS

LIST OF TABLES

Table Page

LIST OF FIGURES

CHAPTER 1
INTRODUCTION

1.1- *Lung Infections in Cystic Fibrosis Patients caused by Pseudomonas aeruginosa*

The simplest scientific definition of a bacterium is a single cellular microorganism (prokaryote) with simple internal structures that lack a nucleus and range in size from 0.2–2.0 nanometers (nm) [1, 2]. Bacteria's size allows these microorganisms to flourish in their environments by forming microcolonies, and this can lead to biofilm formation [3, 4]. The formation of biofilms is an active research area for chemical engineer's because transport phenomena governs' biofilm growth. Studying biofilm formation and maturation of *Pseudomonas aeruginosa* (*P. aeruginosa*) which occurs within the lungs of patients that suffer from Cystic Fibrosis (CF) is an area that is currently under academic research [5, 6].

Short lifespans of CF patients are plagued with symptoms such as frequent lung infections (pneumonia or bronchitis) and shortness of breath [7]. CF is caused by a mutation the gene Cystic Fibrosis Transmembrane Conductance Regulator (CTFR), and this gene controls the flow of salts and fluids in the cell [8, 9]. Mutations in the CTFR gene does not allow mucus from the lungs to be secreted, and this environment is ideal for *P. aeruginosa* which is often the cause for progressive and severe lung disease in CF patients [10, 11]. *P. aeruginosa* forms a biofilm in the lungs and is detrimental because the lungs cannot secrete contaminated sputum and has shown an increased tolerance to antibiotics [12]. Studying *P. aeruginosa's* biofilm growth is done using various techniques such as *in vitro* and *in silico* studies.

1.2 – ***In Vitro Studies of Biofilms***

In vitro methods have been used to study biofilms and consist of three approaches: Closed, Open, and Microcosms [13, 14]. Open studies are dynamic and allow for the quantification of wastes, metabolic byproducts, and dispersed or dead bacteria [13]. The dynamical nature of biofilm growth is governed by transport phenomena, and *in vitro* methods collect data used for *in silico* modeling. *In vitro* methods allow researchers to obtain the complete picture of the necessary steps that lead to biofilm growth.

Open studies of *P. aeruginosa* biofilms have shown that biofilm formation on biotic and abiotic surfaces give resistant to the host's immune defenses and antibiotic medications [15, 16]. These studies have been motivated by CF and has given rise to an understanding of the environmental conditions that contribute to microcolony formation. Environmental factors alter *P. aeruginosa's* metabolism, ultimately causing the bacteria to flourish or perish. Specifically, glucose and lactate are carbon sources metabolized by *P. aeruginosa* and have shown nutrient diversity that aid in the survival of the bacterium [17, 18]. Glucose and lactate are converted to pyruvate which is then metabolized based on the cellular environment (anaerobic/aerobic) [19, 20].

These methods have been important to the field of biofilm research; however, they are also critiqued due to being oversimplistic [13]. One way in which *in vitro* methods are unrealistic is because they are not able to estimate the concentration gradients of most metabolites throughout the biofilm's matrix. To quantify the concentration throughout a biofilm's matrix this is done via a mathematical model because of the size of a biofilm [21]. On average biofilm thickness ranges from 50-400

microns and trying to measure the concentration at this scale with current technologies is impractical [22]. However, microsensors have been used to measure the local oxygen concentration in a defined region of a biofilm [23, 24].

1.3 – *In Silico Studies of Biofilms*

One method that has been used to describe how biofilms mature is referred to as Cellular Automaton (CA), which states that the spatiotemporal variations can only have a finite number of possible states [25]. CA biofilm models generate a wide range of observed biofilm morphologies because they utilize a spatial lattice/grid and it is advantageous because of this ability [25]. The Convection, Diffusion, Reaction and Growth model (CDGR) couples CA with transport phenomena to simulate biofilm growth in environments where fluid is flowing perpendicular to the biofilm. CDRG is a multidimensional model that simulates biofilm maturation, and includes fluid flow over irregular biofilm surfaces, substrate transport by convection and diffusion, substrate consumption, and biomass growth [26]. This is done by combining dynamic equations with CA, which governs the numbers of finite states a biofilm can assume. Boundary conditions that govern the systems dynamics and geometry can be changed which gives CDRG flexibility to simulate a multitude of differing scenarios [26].

A computational technique was developed at the Process Engineering Laboratory at Massachusetts Institute of Technology (M.I.T.) by Jose Gomez, Kai Höffner, and Paul Barton called Dynamic Flux Balance Analysis (DFBAlab) [27, 28]. DFBAlab solves systems of differential equations which have been derived with respect to transport phenomena, but only vary relative to time. This report will describe how transport equations are utilized in DFBAlab to numerically calculate spatiotemporal variations

during biofilm maturation, which is referred to as Spatiotemporal Flux Balance Analysis (SFBA). SFBA will be used to simulate biofilm growth of *P. aeruginosa* by utilizing partial differential equations coupled with a dynamic finite difference grid dependent on the velocity of the biofilm boundary layer. SFBA incorporates solutions from FBA to approximate the bacterial growth rate, metabolite uptake, and metabolite secretion rates for varying compositions [27]. Concentration gradients effect the metabolic network because it is governed by Michaelis-Menten kinetics [29, 30].

1.4 –*Contributions For this Thesis*

An objective of this thesis will be coupling Genome Scale Metabolic Modeling (GSMM) and SFBA with a dynamic boundary condition relative to the biofilm expanding and/or contracting which has never be done, and the coupling of these ideas relative to biofilm expansion makes this thesis novel. Local optima (biomass growth rate, metabolite uptake/secretion rates) from FBA will be used to understand the model bacterium's metabolic response and these parameters will govern their corresponding partial differential equations used in SFBA. The algorithm proposed in this thesis allows for a more accurate portrayal of the physical aspect of biofilm growth. A differential equation that describes the biofilms length is numerically advantageous, because if the biofilm ceases to expand and/or contract the simulation will reach a steady state relative to the length. Spatial dependency of the finite difference grid increases spatial resolution by dividing up the portion of the biofilm where dynamics occurs. Traditionally, the biofilm length is defined as a constant value and space is discretized accordingly. This possesses a problem because the dynamics occurs before and potentially after the defined points, and when the biofilm is starting to grow points that capture the dynamics at the end of the

biofilm are not used. Allowing the finite difference grid to change relative to the length of the biofilm increases spatial resolution and allows this numerical method to concentrate its computational power consistently throughout the biofilm.

CHAPTER 2
REVIEW OF LITERATURE

2.1 –*Genome Scale Metabolic Modeling for Flux Balance Analysis*

Bacterium's metabolic pathways must be defined using GSMM. This model was taken from *Genome-Scale Metabolic Network Analysis of the Opportunistic Pathogen Pseudomonas aeruginosa* for *P. aeruginosa* [31, 32]. FBA is "solved" by constructing a metabolite stoichiometric matrix and used in a Linear Programming (LP) software. LPs are systems of algebraic equations that can take continuous (mixed integer) or discrete (integer) values [33, 34]. Growth rate and metabolite fluxes are continuous because of how they are used to scale the governing partial differential equations (Equations 5,6). For example, on average a typical bacterium's mass is $1x10^{-12}$ grams and depending on the volume under study the density will fluctuate [35]. The LP is solved and the solutions are governed by the cells mass balance which are then used to scale local concentrations. The mass balance was constructed using *P. aeruginosa's* metabolic pathways and was mathematically described by the following equation [36].

$$\frac{dC_i}{dt} = \sum_{j=1}^{r} \lambda_{i,j} \nu_j \tag{1}$$

Equation 1 is a mass balance that can be written for each metabolite (i) in a metabolic pathway. Metabolic pathways consume metabolites produced as a part of metabolic cycles; this is accounted for on the right-hand side (RHS) of Equation 1 by summing over all reactions (r) that produce or consume the metabolite. Metabolite fluxes (ν_j) are scaled by the stochiometric coefficient ($\lambda_{i,j}$) relative to the specific reaction (j) in the metabolic pathway. Given this information a system of differential equations can be constructed with respect to the metabolic pathways.

$$\underbrace{\frac{d}{dt}\begin{bmatrix} C_i \\ \vdots \\ C_M \end{bmatrix}}_{d\underline{X}/dt} = \underbrace{\begin{bmatrix} \lambda_{1,j=1} & \cdots & \lambda_{1,j=r} \\ \vdots & \ddots & \vdots \\ \lambda_{M,j=1} & \cdots & \lambda_{M,j=r} \end{bmatrix}}_{\underline{S}} \underbrace{\begin{bmatrix} v_1 \\ \vdots \\ v_b \end{bmatrix}}_{\underline{v}} - \underbrace{\begin{bmatrix} b_1 \\ \vdots \\ b_M \end{bmatrix}}_{\underline{b}}$$

$$\frac{d\underline{X}}{dt} = \underline{S}\underline{v} - \underline{b} \tag{2}$$

Equation 2 represents the time differential mass balance of an organism's metabolic pathway. This time derivative is set equal to zero stating that the consumption or production of metabolites during the bacteria's metabolic pathway is time independent [37]. This defines the system of differential equations to be a system of algebraic equations which can then be solved as an LP. Gurobi™ is a widely used program that solves LPs and is done by the implementation of a biomass objective function.

$$\underline{S}\underline{v} = \underline{b} = \begin{bmatrix} 0 \\ \vdots \\ 0 \end{bmatrix}$$

$$Z = \sum_{i=1}^{M} C_i v_i \tag{3}$$

$$v_{i,min} < v_i < v_{i,max} \tag{4}$$

Equations 2–4 are used in Gurobi™ to obtain an optimum solution to the set of algebraic equations. Equation 3 is the biomass objective function (Z), and it is the summation of the metabolite fluxes that are being studied in *P. aeruginosa's* metabolism. The objective function is scaled by the weight (C_i) of a particular metabolite [27].

Furthermore, once the LP has found an optimum this gives definite values for the fluxes that maximize the growth rate. These values are consistent with the constrained range and gave insight into how the bacteria will act under varying the maximum metabolite uptake rates. Once FBA has found an optimal solution, the solution can then be used as inputs to scale the differential equations that govern DFBAlab.

2.2 –*Spatiotemporal Modeling of Biofilm Metabolism*

SFBA utilizes partial differential equations along with the corresponding boundary conditions to mathematically characterize biofilm growth. A variety of boundary conditions are used such as convective mass transfer, diffusion, and "no flux", which are used with respect to the environment. To numerically simulate biofilm growth these equations are spatially discretized to relieve the spatial dependency (length of the biofilm) making the equations only time dependent.

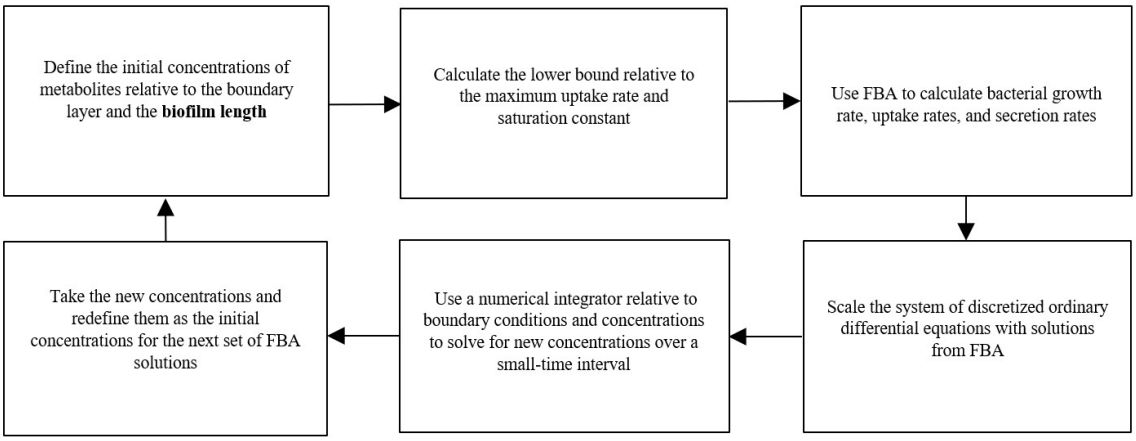

Figure 1: A process flow diagram of Spatiotemporal Flux Balance Analysis.

Figure 1 is a process flow diagram of the algorithm that the numerical method uses to calculate biofilm growth. SFBA uses the bacterium's metabolic pathways defined through GSMM to calculate parameters used to scale the spatially discretized partial differential equations that govern biofilm growth.

Dr. Poonam Phalak in Dr. Michael Henson's group used the fundamental principles of continuum equations in SFBA to model chronic wound biofilm consortium. This spatiotemporal modeling of biofilm metabolisms with *P. aeruginosa* and *Staphylococcus aureus* (*S. aureus*) predicted individual species metabolism and interspecies interaction spatiotemporally with genome-scale resolution [38]. Therefore,

SFBA should be chosen when simulating biofilms that are spatiotemporally dependent, and this thesis adds another level of accuracy to the algorithm by prediction of the biofilm thickness as a function of time as opposed to specifying a constant thickness a priori as in previous work within the Henson group [37, 38, 39, 40].

CHAPTER 3
METHODS

3.1 –*Biofilm Model Formulation*

Model formulation was done using reaction diffusion equations related to transport phenomena, and this states the model does not violate continuum mechanics. The model was derived relative to *in vitro* studies, and this states that at the biofilm-surface interface there is a semipermeable membrane and during expansion the biofilm-air interface has no resistance to expansion (ambient air).

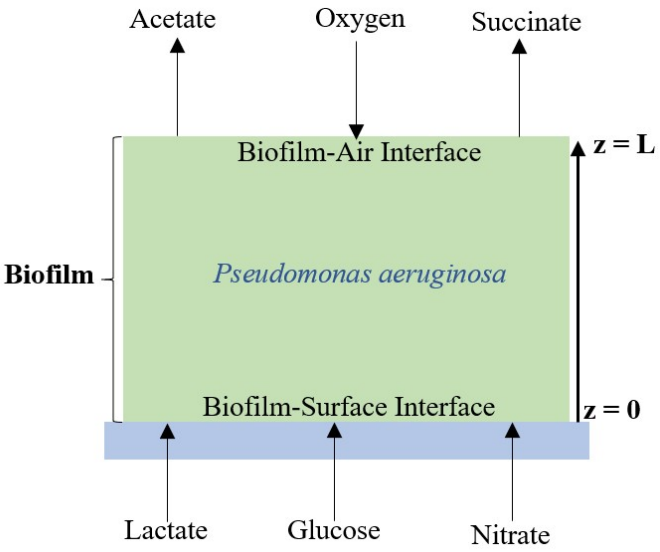

Figure 2: Representation of a biofilm comprised of Pseudomonas aeruginosa [32].

Figure 2 is a representation of the mature state of a biofilm, and for *P. aeruginosa* its essential metabolites are glucose and oxygen [32]. These metabolites allow the bacterium to flourish, but the bacterium has evolved to metabolize lactate and nitrate which is prevalent to survival of the bacterium in varying environments.

$$\frac{\partial X_l}{\partial t} = \mu_l X_l - \mu_d X_l - \frac{\partial}{\partial z}(uX_l) + D_l \frac{\partial^2 X_l}{\partial z^2} \tag{5}$$

$$\frac{\partial M_j}{\partial t} = \upsilon_{M_j,X_i} X_i - \frac{\partial}{\partial z}\left(uM_j\right) + D_{M_j}\frac{\partial^2 M_j}{\partial z^2} \quad (6)$$

Equations 5 and 6 are partial differential equations that describe the concentration gradients of *P. aeruginosa*, glucose, oxygen, acetate, succinate, lactate, and nitrate throughout the biofilm. The RHS of these equations are governed by the change in the diffusive flux and the reaction terms. Equation 5 specifically describes the concentration gradient of *P. aeruginosa* throughout the biofilm, and this equation accounts for growth ($\mu_l X_l$) and death ($\mu_d X_l$) of the bacterium. The replication of the bacterium relies on the growth rate (μ_l) and mortality relies on the death rate (μ_d). Equation 6 describes the metabolites, and the production (υ_{M_j,X_i}) relies on the optimal metabolite fluxes. The next term ($\frac{\partial}{\partial z}(uX_l), \frac{\partial}{\partial z}\left(uM_j\right)$) in Equations 5 and 6 describe how the velocity and velocity gradient effects the concentration gradients. Finally, the last term ($D_l\frac{\partial^2 X_l}{\partial z^2}, D_{M_j}\frac{\partial^2 M_j}{\partial z^2}$) is the change in diffusive flux, which states that diffusion within the biofilm governs the concentration gradients.

Another key part of the model is the boundary conditions that govern the behavior of the equations at the boundaries.

Table 1: Boundary conditions used to govern the corresponding partial differential equations. Each boundary condition relies on how the biomass or metabolites act at the biofilm-surface interface (z = 0) or the biofilm-air interface (z = L) [32].

Species	z = 0	z = L
Biomass	$\partial X_l/_{\partial z} = 0$	$uX_l - D_l\left(\partial X_l/_{\partial z}\right) = k_{m,X_l}[X_l - X_l(L,t)]$
Metabolites	$uM_j - D_{M,j}\left(\partial M_j/_{\partial z}\right) = k_{m,M_j}[M_{j,b} - M_j(z=0,t)]$	$uM_j - D_{M,j}\left(\partial M_j/_{\partial z}\right) = k_{m,M_j}[M_{j,b} - M_j(L,t)]$

Table 1 defines the boundary conditions that govern the partial differential equations at the biofilm-surface and biofilm-air interfaces. Starting at the initial length (z = 0) the no flux boundary condition is applied to *P. aeruginosa* (X_l) because the membrane is impermeable to cells. The metabolites boundary conditions at the biofilm-surface

interface are governed by convective mass transfer, diffusion, and velocity. Metabolites can penetrate the membrane, and this is equal to the convective mass transfer, change in diffusive flux through the biofilm and these are scaled by the velocity of the biofilm boundary layer. At the biofilm-air interface (z = L) *P. aeruginosa* and the metabolites boundary conditions are the same and represent how the velocity of the boundary layer is governed by diffusion and convective mass transfer.

3.2 – ***Simulation of Biofilm Expansion***

Classically the implementation of finite difference is based on defining the area of interest, and in the case of a biofilm it is the length. Without physical knowledge of a biofilm's length, this proposes a problem because biofilms expand and contract stating that the length is not constant. Incorporating a differential equation that describes the expansion and contraction of the biofilm was done to gain another level of accuracy.

$$\frac{du}{dz} = \frac{(\mu_l X_l - \mu_d X_l)}{\rho_{cell}} \tag{7}$$

$$\frac{dL}{dt} = u(t, z) \tag{8}$$

$$L(z, t_i) = L_i \tag{9}$$

Equation 7 describes how the velocity changes throughout the length of the biofilm which is dependent on the local concentration of biomass, growth, and death rate of *P. aeruginosa*. Upon spatial discretization Equation 7 becomes algebraic and is solved simultaneously and the solution is substituted into Equation 8. Equation 8 is then integrated with the system of discretized partial differential equations, ultimately calculating a new length relative to the time interval [32]. Equation 8 is defined as an initial value problem and is governed by the length of the biofilm, which is defined at the starting of the simulation (Equation 9). Once the simulation is executed relative to the

first time step the initial condition is updated by the solution (Equation 8) and the biofilm is spatially re-discretized,

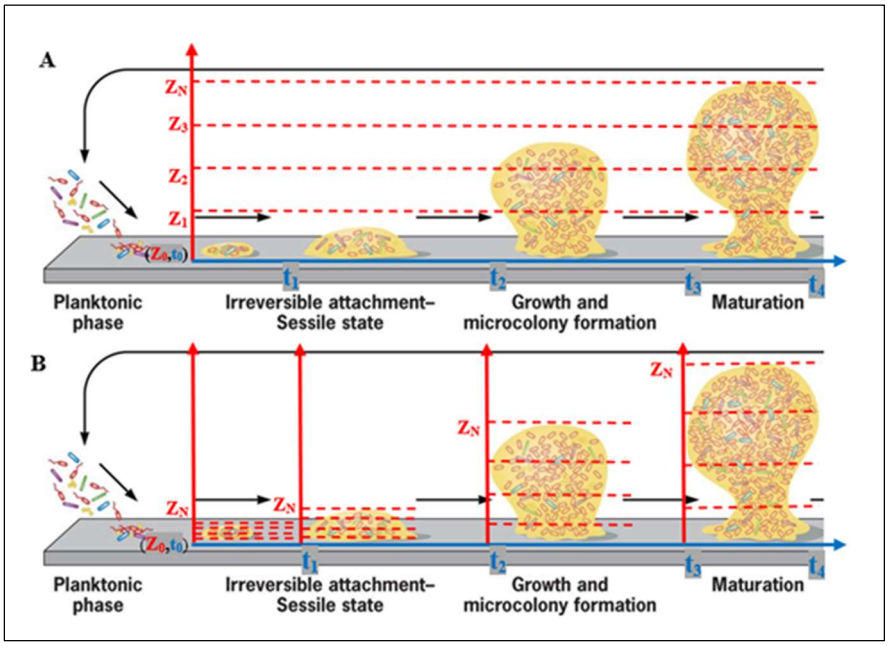

Figure 3: A edited pictorial representation of SFBA utilizing a dynamic finite difference grid. **A** Classical representation of finite difference being applied to biofilm maturation. **B** Novel simulation approach to numerically simulate biofilm maturation [41].

Figure 3A represents how a classical finite difference, and dynamic finite difference (Figure 3B) can be applied to numerically simulate biofilm maturation. Comparing these two methods reveals an obvious advantage based on how space is discretized. Classically the amount of spatial discretization points is fixed over a certain area, and this poses an issue pertaining to the accuracy of the dynamical nature that exists between these points. Thinking of how the governing equations are spatially discretized this implies that during the maturation process not all the equations are used, making the numerical simulation less accurate. Now looking at the dynamic finite difference it shows that space where dynamical growth is taking place is "fully" discretized and this will inherently increase accuracy based on the smaller spatial resolution. Another key characteristic of this model is updating the amount of growth that has taken place with the solution to Equation 8.

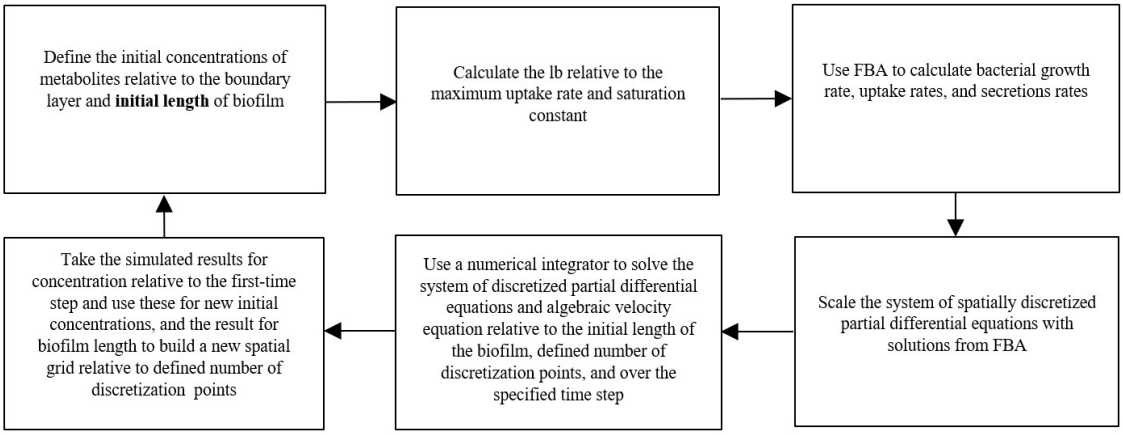

Figure 4: A process flow diagram of Spatiotemporal Flux Balance Analysis that utilizes a dynamic boundary.

Figure 4 is a process flow diagram of the complete algorithm of SFBA with a variable finite difference grid. Initially the user defines the initial concentrations of *P. aeruginosa*, metabolites, initial biofilm length, simulation time, and number of discretization points. A total of 20 discretization points were chosen because it enhanced spatial resolution and adding more points was inconsequential. Simulation times were all chosen to be between 75 and 150 hours, and these were chosen to make sure the biofilm had reached a mature state (pseudo-steady state).

Table 2: Summary of spatiotemporal flux balance analysis parameters used to simulate biofilm maturation with a dynamic finite difference grid [39, 42].

Parameter	Description	Value	Units	Reference
t_{SIM}	Final Simulation Time	75 - 150	hours	Specified
t_{step}	Time Step Interval	1.0	hour	Specified
N_{points}	Number of Spatial Discretization Points	20.0	N/A	Specified
L_0	Initial Biofilm Length	1.0	µm	Specified
u_0	Initial Velocity	0.0	µm/hour	Specified
μ_d	Pseudomonas aeruginosa Death Rate	0.01	1/hour	Fitted
ρ_{cell}	Cell Density	200.0	g/L	Fitted
$[X]_0$	Initial Pseudomonas aeruginosa Concentration Applied at the Biofilm-Surface Interface	1.0	mmol/L	Specified
$[G]_b$	Bulk Glucose Concentration Applied at the Biofilm-Surface Interface	< 20.0, 20.0 , 2.0, 2.0 >	mmol/L	Specified
$[O]_b$	Bulk Oxygen Concentration Applied at the Biofilm-Air Interface	< 0.21, 0.09, 0.21 0.09 >	mmol/L	Specified
D_X	Pseudomonas aeruginosa Diffusion Coefficient	1.00E-10	cm^2/s	Specified
D_G	Glucose Diffusion Coefficient	9.40E-06	cm^2/s	[39]
D_O	Oxygen Diffusion Coefficient	2.68E-05	cm^2/s	[39]
D_A	Acetate Diffusion Coefficient	1.62E-06	cm^2/s	Specified
D_S	Succinate Diffusion Coefficient	1.26E-06	cm^2/s	Specified
D_L	Lactate Diffusion Coefficent	3.54E-06	cm^2/s	[42]
D_N	Nitrate Diffusion Coefficent	1.70E-05	cm^2/s	Specified
$k_{m,G}$	Glucose Mass Transfer Coefficient	2.00E-04	cm/s	Specified
$k_{m,O}$	Oxygen Mass Transfer Coefficient	2.00E-02	cm/s	Specified
$k_{m,A,S}$	Acetate and Succinate Mass Transfer Coefficient	5.00E-04	cm/s	Specified
$k_{m,L,N}$	Lactate and Nitrate Mass Transfer Coefficient	2.00E-03	cm/s	Specified

Table 2 are the defined parameters that were used to simulate *P. aeruginosa* biofilm growth. Various parameters included in this table show benefit to utilizing SFBA with a dynamic finite difference grid. As previously shown in Figure 4 the initial biofilm length was specified at one micron, which encompasses the idea of the simulation starting after the bacterium has formed a microcolony. Mathematically this means that one micron was spatially discretized using 20 node points which increased spatial resolution. Expansion/contraction velocity was initially set to zero to emulate reality. Parameters such as the bulk concentrations, diffusion coefficients, and mass transfer coefficients of the metabolites were defined to enhance biofilm growth and test the simulation based on physical attributes to biofilm maturation. For example, the base case was considered to have a high bulk concentration of glucose (20 mmol/L) and atmospheric dissolved oxygen (0.21 mmol/L) with no initial concentrations of acetate, succinate, lactate, and

nitrate. This allows for the concentrations of glucose and oxygen to be depleted which showed how the biofilm reacted to "starvation." Once the base cases were studied bulk concentrations of nitrate and lactate could be added to see how the biofilm reacted relative to results obtained from FBA.

GSMM is governed by Michaelis-Menten kinetics, which effects the parameters used to scale the partial differential equations. Michaelis-Menten kinetics are functions of the local compositions of metabolites which increased accuracy.

Table 3: Summary of parameters that governed the Michaelis-Menten equation.

Species	K_s	v_{max}
Glucose	0.500	10.0
Oxygen	0.003	20.0
Acetate	0.500	10.0
Succinate	0.500	10.0
Lactate	0.500	10.0
Nitrate	0.005	5.3

Table 3 summarizes the conceptual idea of FBA and gives the need for an upper bound (ub) and lower bound (lb) to find the optima for the biomass objective function. All the upper bounds were set to 1000 mmol/gDW/h which was defined in MATLAB™ [27]. Lower bounds were calculated and were functions of the maximum uptake (υ_{max}) and saturation rates (K_s), and these parameters were taken from previous research [40, 43].

CHAPTER 4
RESULTS AND DISCUSSION

4.1 - *Metabolite Flux Analysis of Pseudomonas aeruginosa*

FBA aids in understanding how the bacterium will grow relative to the metabolite uptake. This is valuable before simulating biofilm growth using SFBA, because FBA shows how the bacterium will react to local compositions of metabolites throughout the biofilm. PA01 iMO1056 genome model was used for FBA [31]. Glucose and oxygen are *P. aeruginosa's* natural metabolites, and this implies that these metabolites will allow the bacterium to replicate [32].

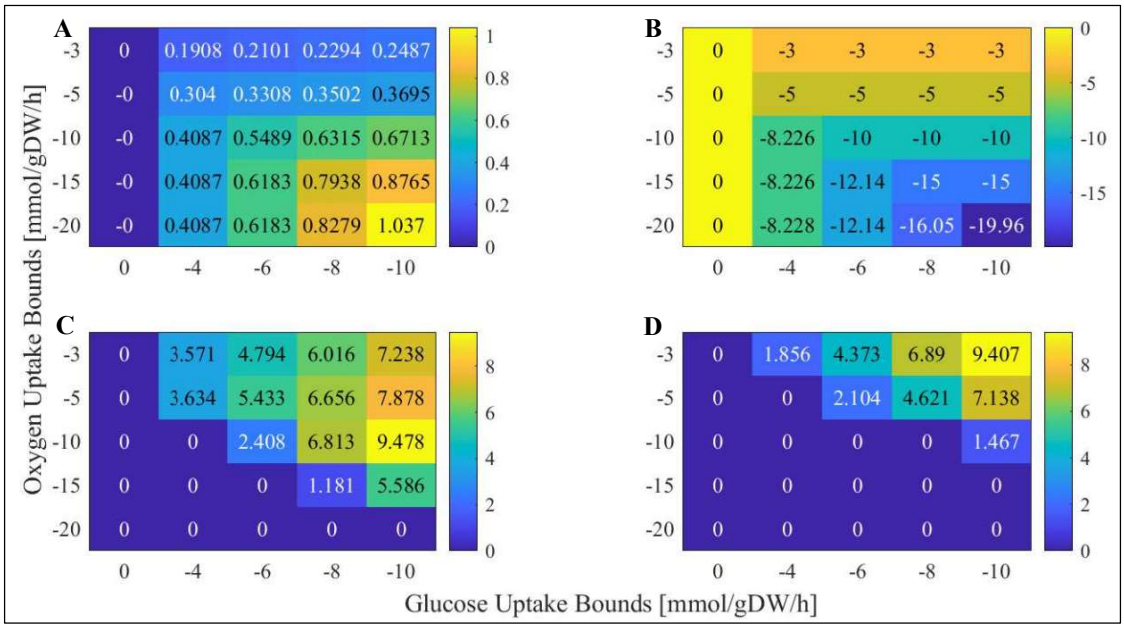

Figure 5: FBA results for *P. aeruginosa* metabolic response to glucose and oxygen uptake. **A** Calculated biomass growth rate [1/h]. **B** Oxygen uptake rate [mmol/gDW/h]. **C** Acetate secretion rate [mmol/gDW/h]. **D** Succinate secretion rate [mmol/gDW/h].

Figure 5 shows that *P. aeruginosa's* growth rate increases and is dependent on the oxygen and glucose uptake. Mathematically the sign of the value dictates whether the value is an uptake rate (−) or secretion rate (+), and that is embedded in the mathematical analysis. Determining the lower uptake bounds was not straight forward, and while running these simulations with no oxygen and glucose the bacterium would show a

minuscule growth rate. Within the genomic model (PA01) the ability for the bacterium to perform anaerobic metabolism is present via nitrate, but no nitrate was being supplied during these simulations [31]. This simulation showed that glucose was always completely metabolized, and the bacterium limited the metabolization of oxygen according to glucose uptake shown in Figure 5B. Prior studies done by Dr. Poonam Phalak and Dr. Michael Henson has shown that *P. aeruginosa* produces acetate and succinate as metabolic byproducts [39]. The study showed that acetate and succinate is produced in anaerobic environments shown in Figures 5C-5D. These results coincide with literature and show that when *P. aeruginosa* is in an anaerobic environment the bacterium produces acetate and succinate via pyruvate fermentation [44, 45, 46].

FBA utilizing glucose and oxygen uptake is the base case in this study because of *P. aeruginosa's* "natural" metabolic pathways. However, *P. aeruginosa* has shown nutrient diversity based on its ability to evolve to survive in its current environment [47, 48, 49]. The first evolutionary step that was studied was the ability for the bacterium to metabolize lactate (carbon source) [50].

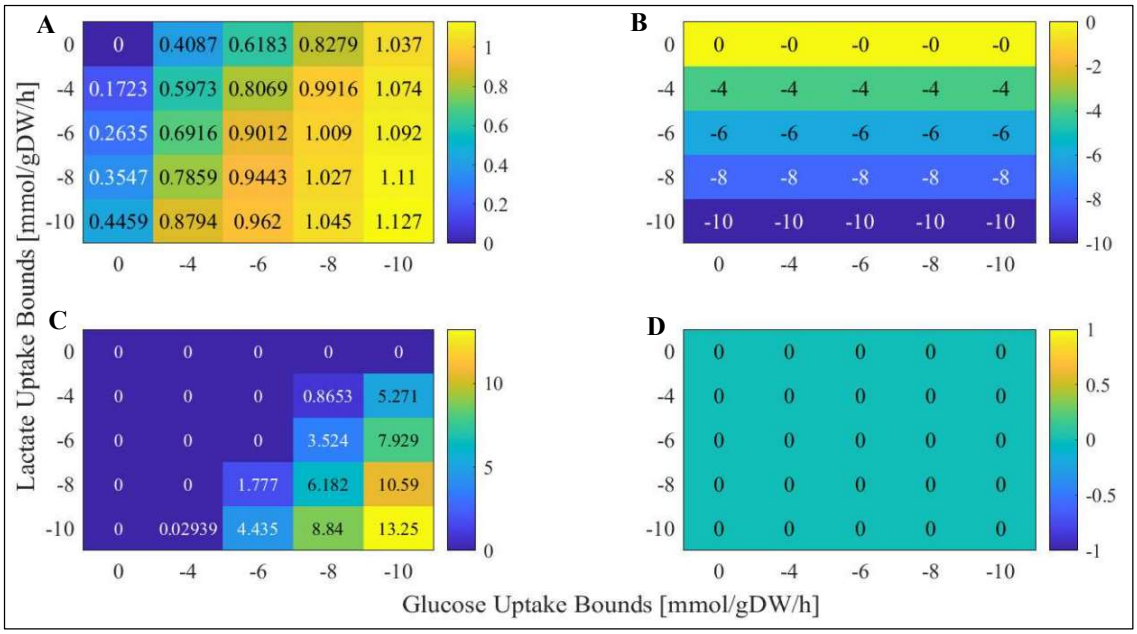

Figure 6: FBA results for *P. aeruginosa* metabolic response to glucose, lactate, and oxygen uptake. **A** Calculated biomass growth rate [1/h]. **B** Lactate uptake rate [mmol/gDW/h]. **C** Acetate secretion rate [mmol/gDW/h]. **D** Succinate secretion rate [mmol/gDW/h].

Figure 6 shows how the bacterium reacted to glucose and lactate uptake at a constant oxygen uptake rate (-20 mmol/gDW/h). Minimally, increasing the amount of carbon sources should increase the total biomass growth rate. This phenomenon is shown in Figure 6A, and portrays the bacterium and FBA is behaving according to previous studies [48]. Lactate uptake was always maximized to the bound which shows that the bacterium has evolved relative to glucose poor environments. Now in question is the ability for the bacterium to produce acetate and succinate as metabolic byproducts. Figures 6C-6D show that lactate has an inversely affected anerobic production of acetate and made succinate production cease.

Finally, the last variation studied relative to *P. aeruginosa's* evolutionary advantage is the metabolism of nitrate [51, 52]. This studied was aimed to understand how the bacterium reacted under anerobic environments.

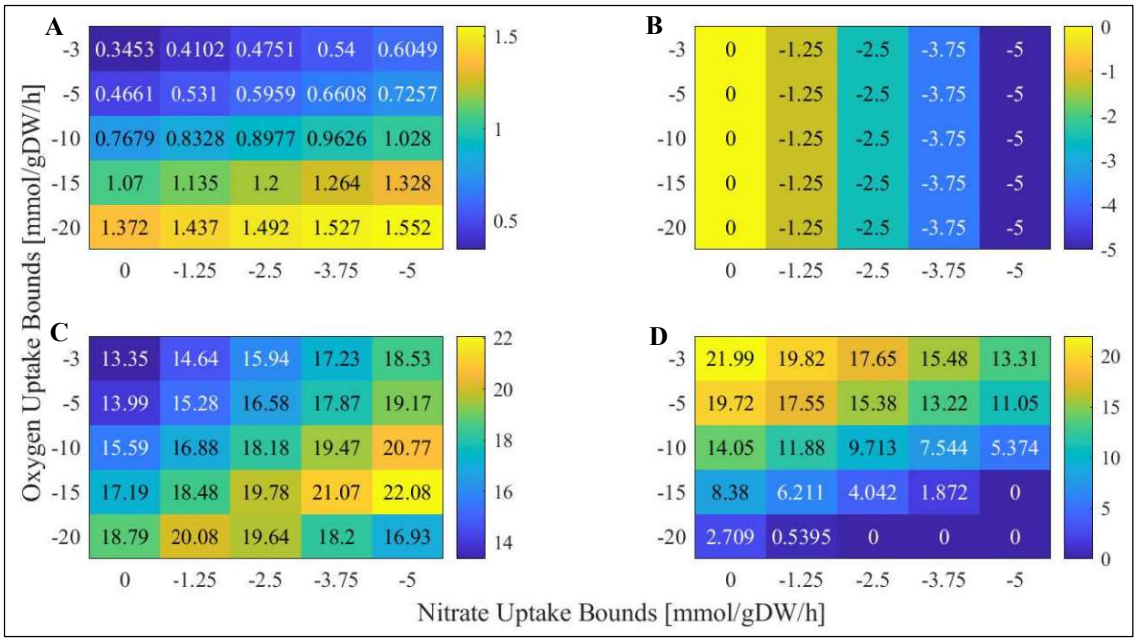

Figure 7: FBA results for *P. aeruginosa* metabolic response to glucose, nitrate, and oxygen uptake. **A** Calculated biomass growth rate [1/h]. **B** Nitrate uptake rate [mmol/gDW/h]. **C** Acetate secretion rate [mmol/gDW/h]. **D** Succinate secretion rate [mmol/gDW/h].

Figure 7 shows how the bacterium reacted to oxygen, and nitrate uptake relative to a fixed glucose uptake (-10 mmol/gDW/h). Specifically, the biomass growth rate increased with the maximum oxygen and nitrate uptake rate bounds. Figure 7B shows that the bacterium will uptake all available nitrate and is not reliant on oxygen uptake. Nitrate uptake during low oxygen uptake states the bacterium will replicate in low oxygen environments. Figures 7C-7D show the acetate and succinate secretion rate, and these rates follow the same trend, but the secretion rates increased due to *P. aeruginosa's* metabolic pathways.

4.2 - ***Pseudomonas aeruginosa Biofilm Growth***

The main objective of this thesis is to use SFBA with a finite difference grid that varied spatiotemporally. The equations and algorithm have been previously stated, and these results were simulated with parameters that are included in Table 2 and Table 3.

SFBA simulations were done with the notion of reaching a pseudo-steady state concentration of biomass and metabolites throughout the biofilm. This aided in understanding how the concentration of biomass and metabolites varied with time and behaved at the two boundaries.

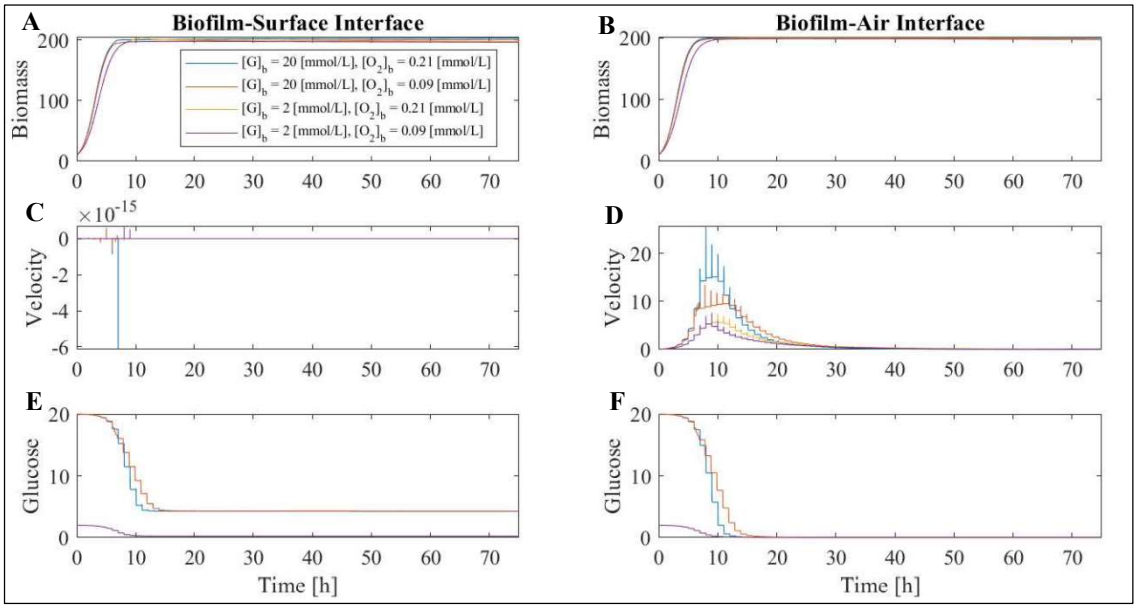

Figure 8: SFBA predictions of time variations for *P. aeruginosa* biofilm growth for different supplied glucose and oxygen concentrations ($[G]_B$ = 20 mmol/L $[O_2]_B$ = 0.21 mmol/L, $[G]_B$ = 20 mmol/L $[O_2]_B$ = 0.09 mmol/L, $[G]_B$ = 2 mmol/L $[O_2]_B$ = 0.21 mmol/L, $[G]_B$ = 2 mmol/L $[O_2]_B$ = 0.09 mmol/L) respectively. **A** *P. aeruginosa* biofilm-surface interface temporal concentration [g/L]. **B** *P. aeruginosa* biofilm-air interface temporal concentration [g/L]. **C** Variations in axial velocity at biofilm-surface interface [µm/h]. **D** Variations in axial velocity at biofilm-air interface [µm/h]. **E** Glucose temporal concentration at biofilm-surface interface [mmol/L]. **F** Glucose temporal concentration at biofilm-air interface [mmol/L].

Figure 8 are results of biofilm simulation over a duration of 75 hours, and this simulation time was chosen for reassurance of reaching a pseudo-steady state (mature biofilm). Two sections of the biofilm were plotted to show how the metabolites and axial velocity of the boundary behaved, and four different supplied concentrations of glucose and oxygen at the boundaries were simulated. Figure 8A-8B are simulated results of the biomass concentration at the biofilm-surface and biofilm-air interface, respectively. Both plots

show exponential growth in biomass during the first 10 hours of simulation which is directly correlated with the metabolization of glucose and oxygen. Axial velocity of the biofilm boundary was calculated using Equation 8. Figure 8C is how the axial velocity behaved at the biofilm-surface interface, which is governed by the no flux boundary condition. Figure 8D shows that the biofilm showed peak expansion during the first ten hours, and then started to decrease as the biomass reached steady state. Behavior of biomass and velocity should be governed by the local concentrations of glucose and oxygen at the boundaries and throughout the biofilm. Figure 8E-8F shows how glucose is consumed over the duration of the simulation at the boundary. Both plots show that glucose is consumed during the first 10 hours, except at the biofilm-surface interface with high bulk concentrations (20 mmol/L).

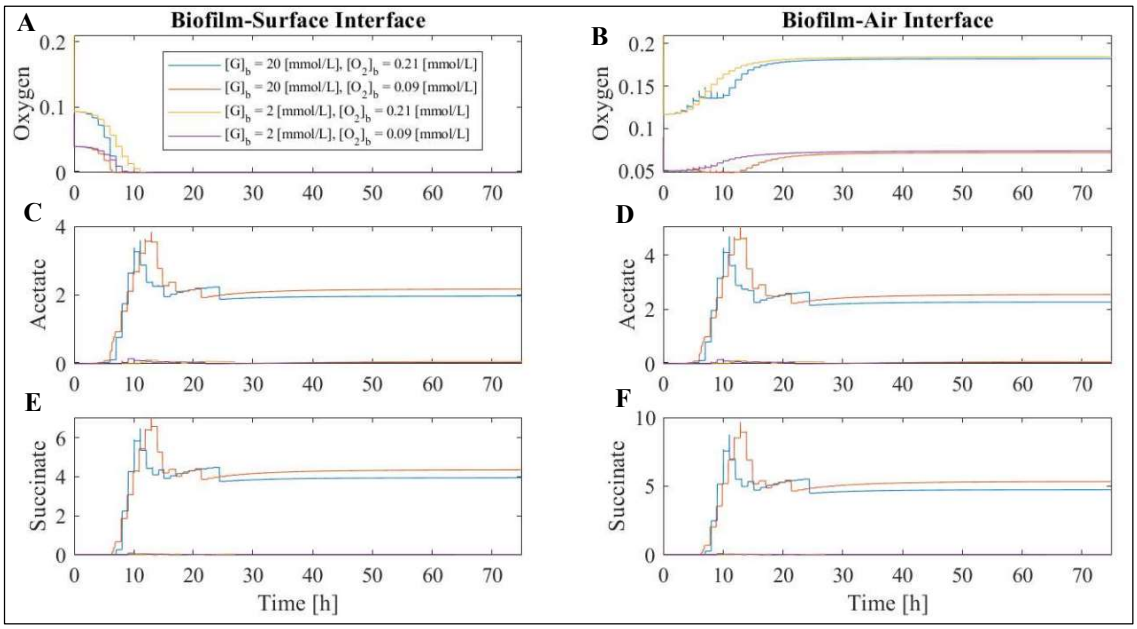

Figure 9: SFBA predictions of time variations for *P. aeruginosa* biofilm growth for different supplied glucose and oxygen concentrations. **A** Oxygen temporal concentration at the biofilm-surface interface [mmol/L]. **B** Oxygen temporal concentration at the biofilm-air interface [mmol/L]. **C** Acetate temporal concentration at the biofilm-surface interface [mmol/L]. **D** Acetate temporal concentration at the biofilm-air interface [mmol/L]. **E** Succinate temporal concentration at the biofilm-surface interface [mmol/L]. **F** Succinate temporal concentration at the biofilm-air interface [mmol/L].

Figure 9 contains the simulation results of oxygen, acetate, and succinate. Figures 9A-9B show the concentration gradients of oxygen throughout the simulation. Specifically, Figure 9A shows that oxygen is completely depleted and is not dependent on the bulk glucose concentration. Oxygen depletion explains why glucose was not fully consumed at the biofilm-surface interface in Figure 8E. Figures 9C-9F show that acetate and succinate were produced when the local composition of oxygen was low in the biofilm which corresponds to simulation results from FBA.

The spatiotemporal variation for the axial velocity governs the dynamic finite difference grid, and this implies that the biofilm thickness is calculated after every time step within the simulation. Figure 10 shows that the bulk concentration of glucose is the determining factor for the maximization of biofilm thickness. It also shows that having a higher bulk concentration of oxygen allows for the biofilm to become thicker but is less significant compared to glucose.

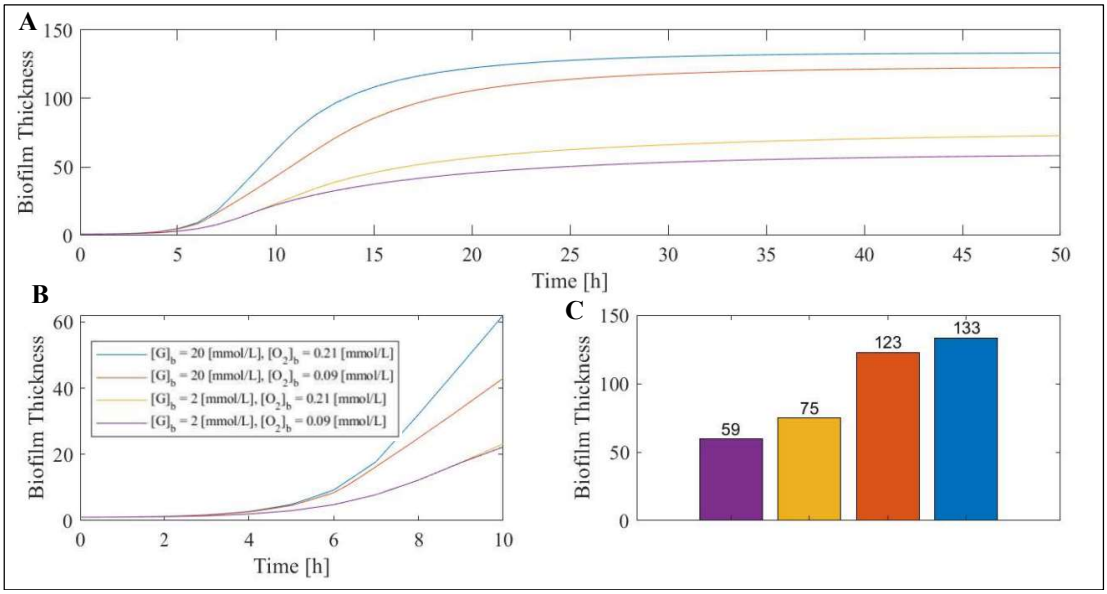

Figure 10: SFBA predictions of biofilm thickness for different supplied glucose and oxygen concentrations. **A** Biofilm thickness after a fifty-hour simulation. **B** Biofilm thickness after the first twenty hours of simulation. **C** Pseudo-steady state biofilm thicknesses at fifty hours for varying bulk concentrations of glucose and oxygen.

Figures 8-10 have shown how the velocity, biomass, and metabolites have varied with respect to time. These analyses do not show spatial variations within the biofilm. Therefore, the velocity, biomass concentrations, and metabolite concentrations were plotted as a function of position.

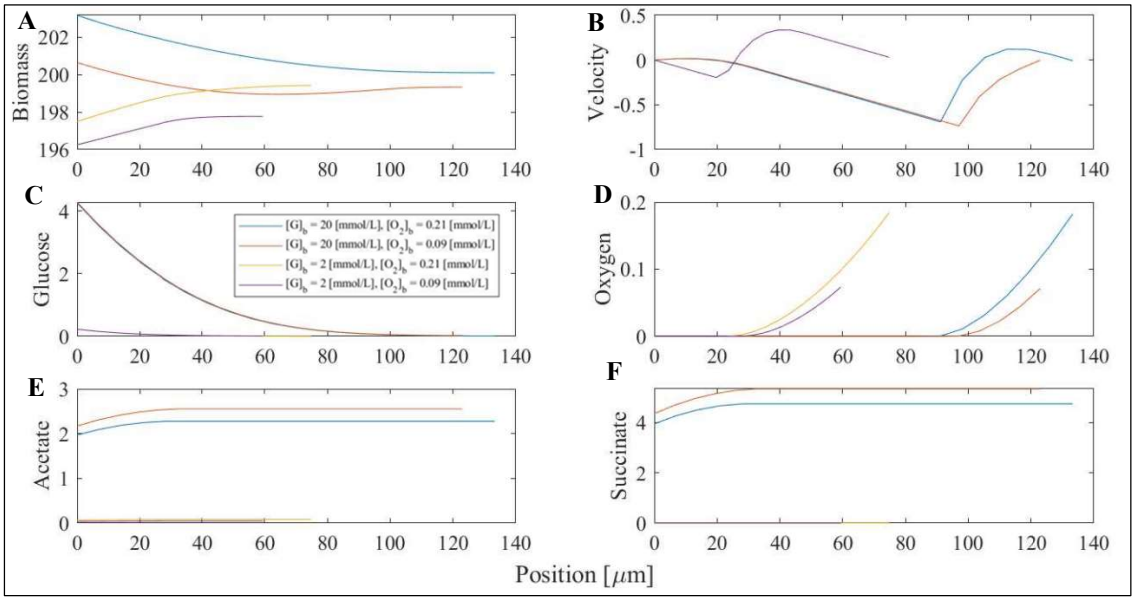

Figure 11: SFBA predictions of spatial gradients for different supplied glucose and oxygen concentrations. **A** Spatial biomass concentrations [g/L]. **B** Axial velocities [μm/h]. **C** Spatial concentration of glucose [mmol/L]. **D** Spatial concentration of oxygen [mmol/L]. **E** Spatial concentration of acetate [mmol/L]. **F** Spatial concentration of succinate [mmol/L].

Specifically, the noticeable difference in Figure 11 is during high and low bulk glucose concentrations. When glucose is in excess *P. aeruginosa* concentration decreases slightly as the biofilm length increases, and when glucose is not in excess *P. aeruginosa's* concentration increases as the biofilm thickens. This is because the concentration of the essential metabolites and where they are prominent. Glucose is supplied at the base (Position = 0) and this metabolite is the essential carbon containing compound that is oxidized, and for the case of high glucose concentration the bacterium metabolizes the oxygen at a higher rate. On the other hand, when the glucose bulk concentration is low,

we see an increase in the concentration of *P. aeruginosa*, and this is due to the ability to completely metabolize glucose throughout the biofilm.

FBA was used to calculate the parameters that served as inputs to scale the discretized partial differential equations. Figure 12 are the calculated parameters as a function of position in the biofilm. Figure 12A shows that the biomass growth rate never becomes zero which implies the bacterium is always growing, because of local growth through the combined uptake of glucose and oxygen. Figure 12B states that glucose does not limit the ability for the bacterium to replicate and growth is reliant on oxygen uptake. Figures 12D-12E follow the same trend as FBA, which when oxygen uptake is limited the secretion rate of acetate and succinate are maximized.

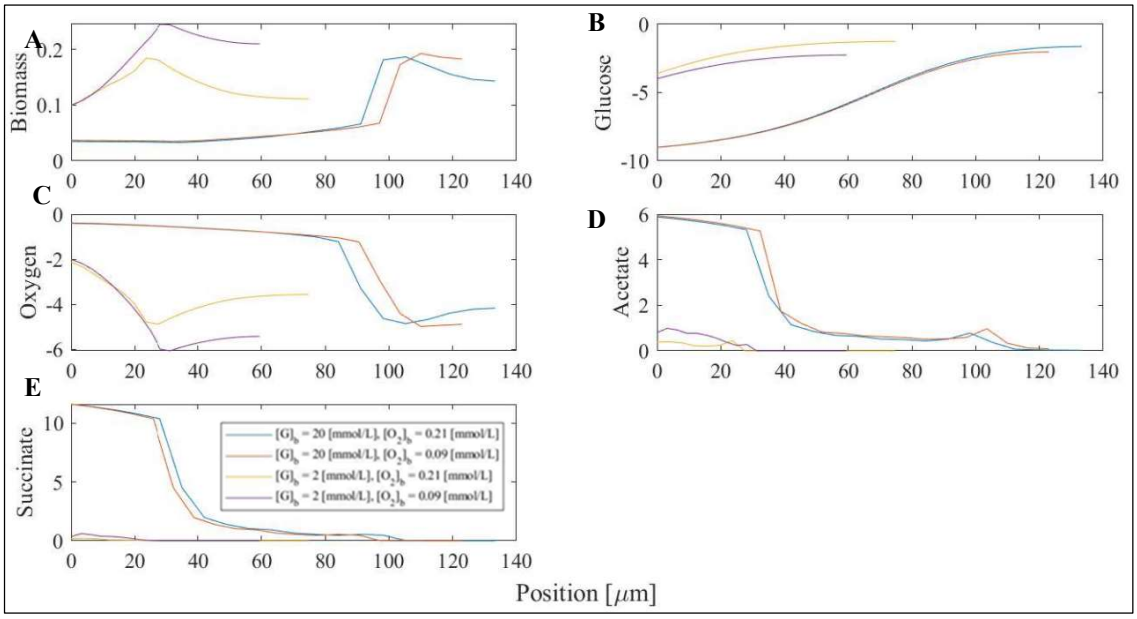

Figure 12: SFBA predictions for the calculated growth rate and metabolite fluxes relative to the position in the biofilm for different supplied glucose and oxygen concentrations **A** Spatially distributed biomass growth rate [1/h]. **B** Spatially distributed glucose uptake rate [mmol/gDW/h]. **D** Spatially distributed oxygen uptake rate [mmol/gDW/h]. **E** Spatially distributed acetate secretion rate [mmol/gDW/h]. **F** Spatially distributed succinate secretion rate [mmol/gDW/h].

FBA predicted that *P. aeruginosa* can replicate via the metabolization of glucose and lactate. This phenomenon was also studied using SFBA governed by a dynamic finite difference grid.

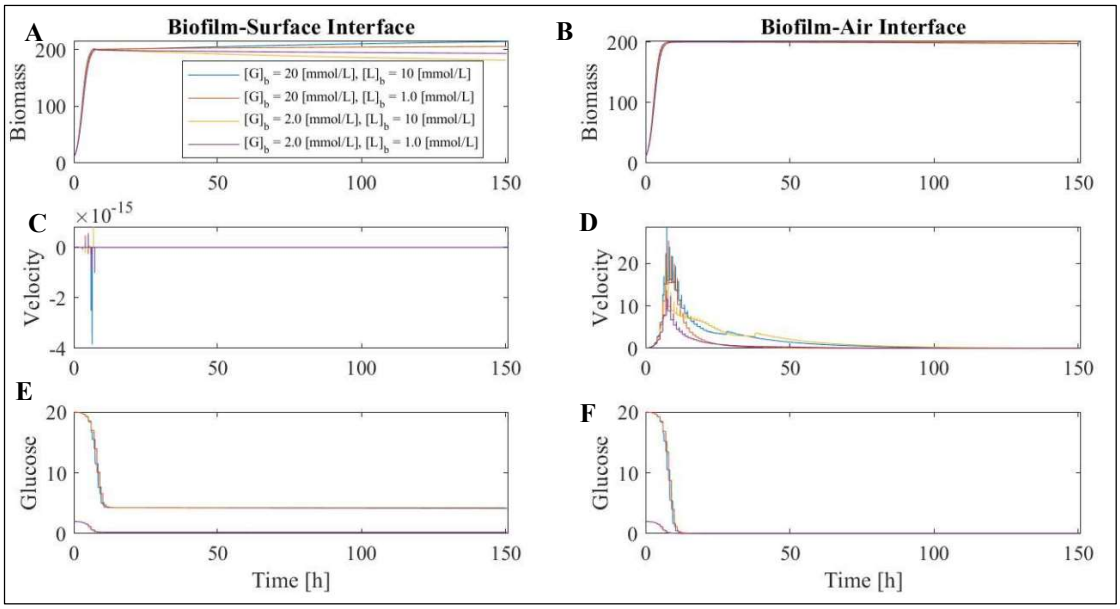

Figure 13: SFBA predictions of time variations for *P. aeruginosa* biofilm growth for different supplied glucose, lactate, and oxygen concentrations ($[G]_B$ = 20 mmol/L $[L]_B$ = 10 mmol/L, $[G]_B$ = 20 mmol/L $[L]_B$ = 1.0 mmol/L, $[G]_B$ = 2.0 mmol/L $[L]_B$ = 10 mmol/L, $[G]_B$ = 2.0 mmol/L $[L]_B$ = 1.0 mmol/L) respectively. **A** *P. aeruginosa* biofilm-surface interface temporal concentration [g/L]. **B** *P. aeruginosa* biofilm-air interface temporal concentration [g/L]. **C** Variations in axial velocity at biofilm-surface interface [μm/h]. **D** Variations in axial velocity at biofilm-air interface [μm/h]. **E** Glucose temporal concentration at biofilm-surface interface [mmol/L]. **F** Glucose temporal concentration at biofilm-air interface [mmol/L].

Figure 13 contains 150-hour simulation results for varying the supplied concentrations of glucose and lactate, while holding the bulk oxygen concentration constant (0.21 mmol/L). Figure 13A shows that the concentration of lactate has a negligible effect compared to glucose at the biofilm-surface interface. Biomass at the biofilm-air interface (Figure 13B) shows that lactate is inconsequential on the pseudo-steady state biomass concentration. Axial velocity and glucose show the same trends at both interfaces as the previous simulation (Figures 13C-13F).

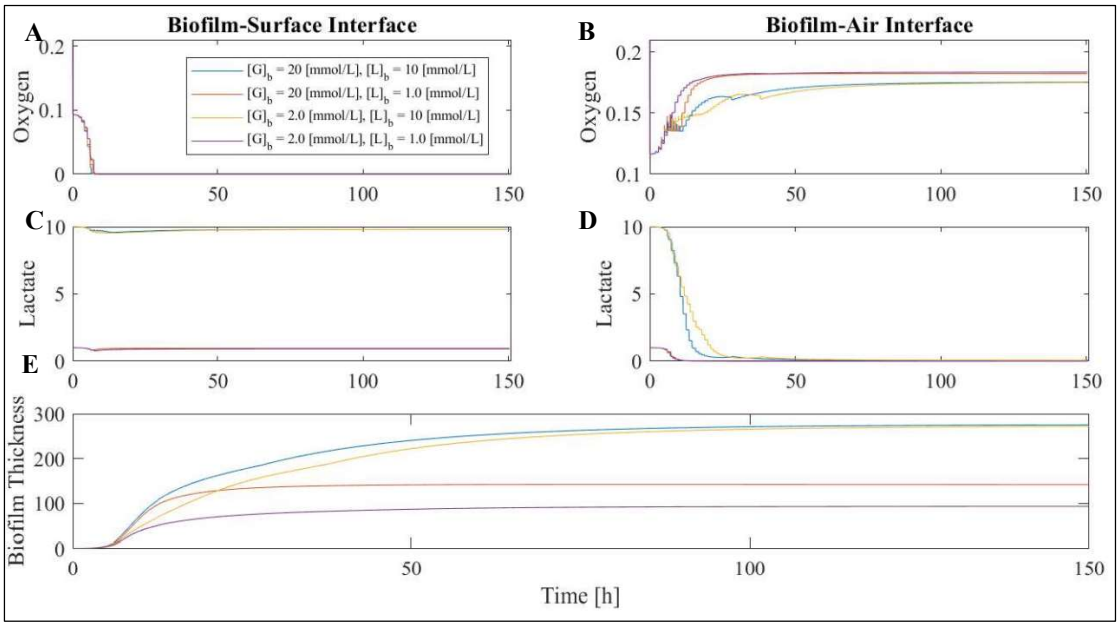

Figure 14: SFBA predictions of time variations for *P. aeruginosa* biofilm growth for different supplied glucose, lactate, and oxygen concentrations. **A** Oxygen temporal concentration at the biofilm-surface interface [mmol/L]. **B** Oxygen temporal concentration at the biofilm-air interface [mmol/L]. **C** Lactate temporal concentration at the biofilm-surface interface [mmol/L]. **D** Lactate temporal concentration at the biofilm-air interface [mmol/L]. **E** Biofilm thickness after a 150-hour simulation.

Figure 14 are the simulated results of oxygen, lactate, and biofilm thickness. Comparing Figure 9A to Figure 14A the consumption of oxygen in the presence of lactate at the biofilm-surface interface is depleted at the same rate and is not specifically dependent on the concentrations of glucose. Figure 9B and Figure 14B shows that the presence of lactate aids in oxygen consumption at the biofilm-air interface. Figures 14C-14D shows that lactate is not completely consumed until an excess of oxygen is available (biofilm-air interface). The biomass growth rate increased by increasing glucose and lactate uptake (Figure 6), and this is shown in comparing Figure 10 to Figure 13E. Lactate is supplied at the biofilm-surface interface which caused the biofilm thickness to increase without respect to the glucose concentration.

Concentrations relative to the position in the biofilm were also plotted to understand how introducing lactate effected the local concentration.

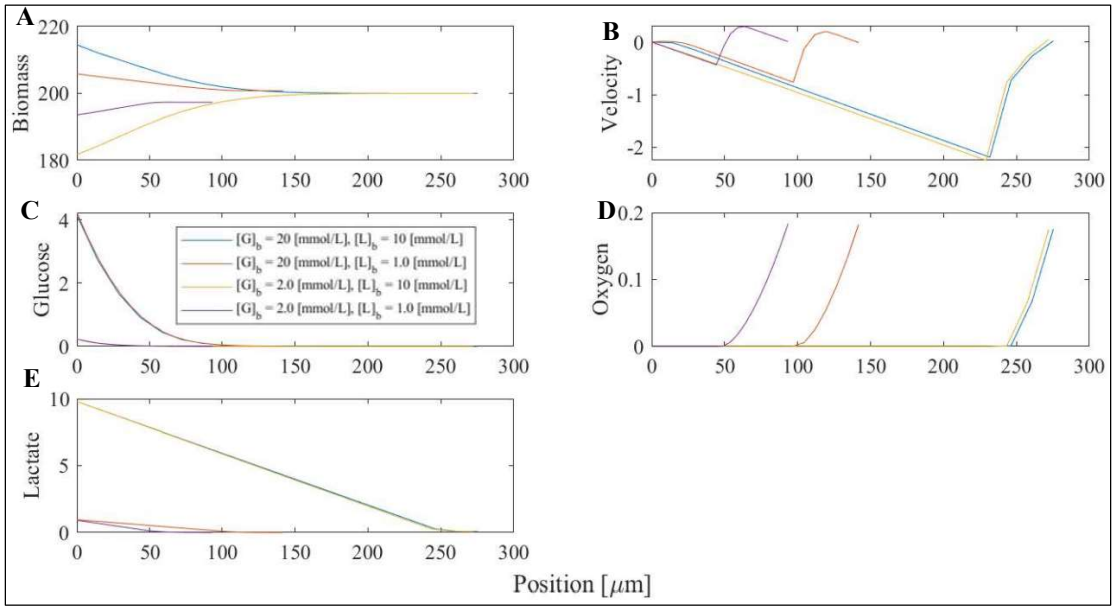

Figure 15: SFBA predictions of spatial gradients for different supplied glucose, lactate, and oxygen concentrations. **A** Spatial biomass concentration [g/L]. **B** Axial velocities [μm/h]. **C** Spatial concentration of glucose [mmol/L]. **D** Spatial concentration of oxygen [mmol/L]. **E** Spatial concentration of lactate [mmol/L].

Starting with the biomass concentration, when comparing Figure 11A to Figure 15A shows similar trends except for low glucose and low lactate bulk concentrations (purple line). The biomass concentration is higher relative to position because of the length of the biofilm, which increases oxygen permeability (Figure 15D). Comparing the axial velocity from figure 11B to figure 15B shows that the bulk concentration of glucose determines the axial velocities behavior. Another noticeable difference was the local oxygen concentration throughout the biofilm. Figure 11C and Figure 15D show a similar trend when oxygens concentration is depleted. Lastly, the concentrations of lactate showed linear profiles, which mathematically stated the gradients are governed by diffusion [32]. Bulk concentrations of lactate increased the magnitude throughout the biofilm, but the trends were similar regarding diffusional limitations.

The last evolutionary advantage studied was supplying nitrate at the biofilm-surface interface. As before these results will be compared to the base case to see how this metabolite altered biofilm maturation,

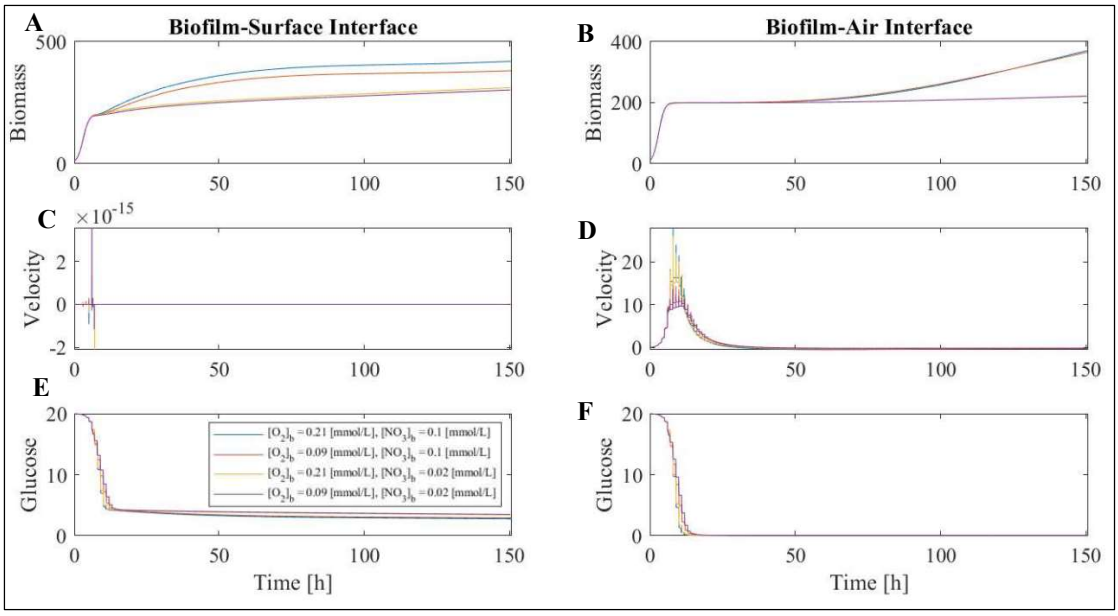

Figure 16: SFBA predictions of time variations for *P. aeruginosa* biofilm growth for different supplied glucose, nitrate, and oxygen concentrations ($[O_2]_B$ = 0.21 mmol/L $[N]_B$ = 0.01 mmol/L, $[O_2]_B$ = 0.09 $[N]_B$ = 0.1 mmol/L, $[O_2]_B$ = 0.21 $[N]_B$ = 0.02 mmol/L, $[O_2]_B$ = 0.02 $[N]_B$ = 0.02 mmol/L) respectively. **A** *P. aeruginosa* biofilm-surface interface temporal concentration [g/L]. **B** *P. aeruginosa* biofilm-air interface temporal concentration [g/L]. **C** Variations in axial velocity at biofilm-surface interface [μm/h]. **D** Variations in axial velocity at biofilm-air interface [μm/h]. **E** Glucose temporal concentration at biofilm-surface interface [mmol/L]. **F** Glucose temporal concentration at biofilm-air interface [mmol/L].

Comparing Figure 8A to Figure 16A shows a significant increase in the biomass concentrations from introducing nitrate. Nitrate promotes metabolism at the biofilm-surface interface and oxygen promotes metabolism at the biofilm-air interface. Axial velocity behaves the same as the base case with no significant increase in the peak at the biofilm-air interface. Increases in the biomass concentrations should be correlated with a sharp depletion of glucose, however, when comparing the base case (Figures 8E-8F) to supplying a bulk nitrate concentration (Figures 16E-16F) the glucose time profiles are

similar. This paradox is because of the nitrate concentration profile, which is included in Figure 17.

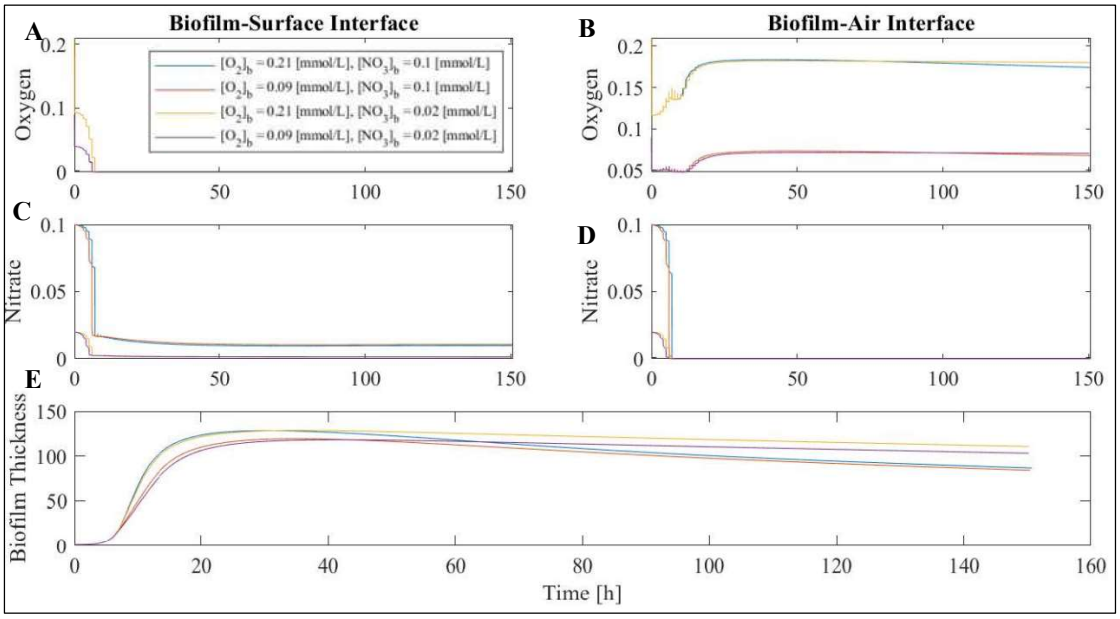

Figure 17: SFBA predictions of time variations for *P. aeruginosa* biofilm growth for different supplied glucose, nitrate, and oxygen concentrations. **A** Oxygen temporal concentration at the biofilm-surface interface [mmol/L]. **B** Oxygen temporal concentration at the biofilm-air interface [mmol/L]. **C** Nitrate temporal concentration at the biofilm-surface interface [mmol/L]. **D** Nitrate temporal concentration at the biofilm-air interface [mmol/L]. **E** Biofilm thickness after a 150-hour simulation.

Throughout this study oxygen has been limited at the biofilm-surface interface which agrees with this simulation (Figure 17A). Nitrate being supplied at the biofilm-surface interface should aid in the consumption of glucose, but Figure 17C shows that nitrate is consumed at the same rate of oxygen, and this explained why the time profile of glucose were similar. Oxygen and nitrate at the biofilm-air interface (Figures 17B,17D) shows that each metabolite is consumed relatively quickly which agrees with all the previous results. An anomaly that did occur was in the biofilm thickness (Figure 17E) which increases exponentially during the first period of simulation but starts to fall as the

simulation continues. This is due to the local composition of glucose because it is the limiting metabolite at the biofilm-air interface.

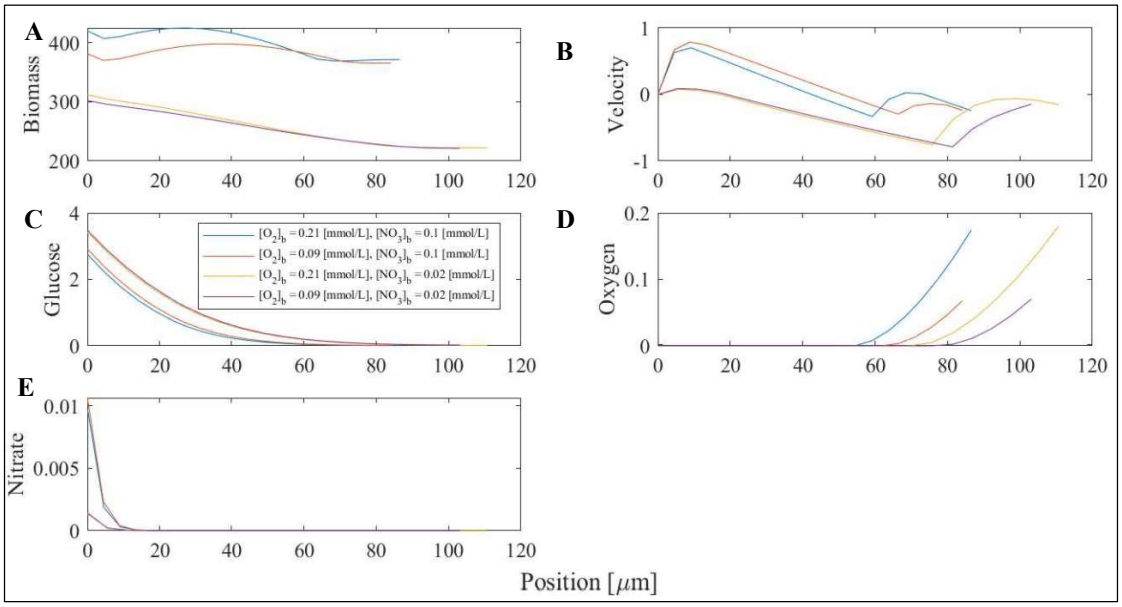

Figure 18: SFBA predictions of spatial gradients for different supplied glucose, nitrate, and oxygen concentrations. **A** Spatial biomass concentration [g/L]. **B** Axial velocities [μm/h]. **C** Spatial concentration of glucose [mmol/L]. **D** Spatial concentration of oxygen [mmol/L]. **E** Spatial concentration of nitrate [mmol/L].

Figure 18 is the spatial profiles of the velocity and metabolites throughout the biofilm relative to a supplied concentration of nitrate at the biofilm-surface interface. Biomass concentrations at the biofilm-surface interface (Figure 18A) shows a significant increase compared to the base case (Figure 11A), and these results coincide with previous results. Figure 18B shows a positive steady state axial velocity for a duration of the numerical study (≈ 10 microns) which deviated from the previous studies. This is due to the rapid growth of *P. aeruginosa* which caused the boundary layer to reach a net positive axial velocity for those specific time intervals. Figures 18C-18D show similar profiles to the previous studies. Finally, Figure 18E depicts how the concentration gradient of nitrate is depleted within the first 10 microns of the biofilm, which allows the biofilm to flourish at the biofilm-surface interface.

These studies have all shown a similar trend when viewing biofilm growth in terms of metabolites and where they are supplied. Base cases showed that as the biofilm expands the concentration of oxygen becomes the limiting metabolite. Introducing lactate to the biofilm-surface interface followed a similar trend to the base case because of the inability for glucose and lactate to be metabolized simultaneously. Furthermore, introducing nitrate at the boundary allowed the bacterium to replicate and stay "dense" at the interface, but as the biofilm grew cells were also limited by oxygen diffusion from the biofilm-air interface. These result state a logical physical definition of what would alter biofilm growth *in vitro*. Since these results mimic reality, they are conclusive examples of this novel approach to incorporate GSMM and SFBA with a dynamic finite difference to calculate the length of the biofilm to be adequate.

CHAPTER 5
FUTURE WORK

Utilization of SFBA relative to a dynamic finite difference grid has simulated idealistic results. *P. aeruginosa's* GSMM was used to compute governing parameters used by the governing partial differential equations. To obtain a more accurate picture of metabolism the cell death rate could be added to FBA that is embedded within this numerical simulation. Making the cell death rate a function of the biomass objective function would make the model more mathematically fit. *P. aeruginosa* has a broad range of metabolites as well, and it has been shown that the bacterium can metabolize acetate and succinate. Utilizing all metabolites uptakes and using them efficiently (with respect to computational time) is another goal that would be done via the biomass objective function.

Additionally, adding higher dimensionality to the governing partial differential equations would allow for an more accurate result of the concentration gradients within the biofilm. Adding width (x) and depth (y) to the numerical simulation would allow for the simulation to take on *in vitro* laboratory studies. Increasing spatial resolution would logically coincide with similar boundary layer analyses (biofilm-air interface). To construct a simulation in this matter the biofilm boundary layer would have a velocity in three directions, which would add more equations that are spatially discretized and generate a very computationally demanding biofilm model. During the construction of a high dimensional model, data for this simulation could be obtained through *in vitro* studies allowing for a more detailed comparison. In turn the *in vitro* data can also be taken to support the higher dimensional model.

REFERENCES

1. Vidyasagar, A. (2019, April 25). What Are Bacteria? LiveScience. https://www.livescience.com/51641-bacteria.html.
2. Bacteria - Definition, Shapes, Characteristics, Types & Examples. Biology Dictionary. (2019, October 4). https://biologydictionary.net/bacteria/.
3. Bacteria - Size, Shape and Arrangement. MicroscopeMaster. (2021, June 12). https://www.microscopemaster.com/bacteria-size-shape-arrangement.html.
4. Donlan, R. M. (2000). Role of biofilms in antimicrobial resistance. ASAIO journal, 46(6), S47-S52.
5. Bhagirath, A. Y., Li, Y., Somayajula, D., Dadashi, M., Badr, S., & Duan, K. (2016). Cystic fibrosis lung environment and Pseudomonas aeruginosa infection. *BMC pulmonary medicine*, 16(1), 1-22.
6. Research We Fund. CF Foundation. (2021, June 12). https://www.cff.org/Research/About-Our-Research/Research-We-Fund/.
7. About Cystic Fibrosis. CF Foundation. (2021, August 12). https://www.cff.org/What-is-CF/About-Cystic-Fibrosis/.
8. WebMD. (2021, June 12). Cystic Fibrosis (CF): Symptoms, Causes, Diagnosis, Treatment. WebMD. https://www.webmd.com/children/what-is-cystic-fibrosis.
9. Tsui, L. C. (1992). Mutations and sequence variations detected in the cystic fibrosis transmembrane conductance regulator (CFTR) gene: a report from the Cystic Fibrosis Genetic Analysis Consortium. Human mutation, 1(3), 197-203.
10. Silva, P. (2018, July 18). Pseudomonas aeruginosa. Cystic Fibrosis News Today. https://cysticfibrosisnewstoday.com/pseudomonas-aeruginosa/.
11. Ziedalski, T. M., Kao, P. N., Henig, N. R., Jacobs, S. S., & Ruoss, S. J. (2006). Prospective analysis of cystic fibrosis transmembrane regulator mutations in adults with bronchiectasis or pulmonary nontuberculous mycobacterial infection. *Chest*, 130(4), 995-1002.
12. Høiby, N., Ciofu, O., & Bjarnsholt, T. (2010). Pseudomonas aeruginosa biofilms in cystic fibrosis. *Future microbiology*, *5*(11), 1663-1674.
13. Lebeaux, D., Chauhan, A., Rendueles, O., & Beloin, C. (2013). From in vitro to in vivo models of bacterial biofilm-related infections. Pathogens, 2(2), 288-356.
14. Salli, K. M., & Ouwehand, A. C. (2015). The use of in vitro model systems to study dental biofilms associated with caries: a short review. *Journal of oral microbiology*, 7(1), 26149.
15. Pericolini, E., Colombari, B., Ferretti, G., Iseppi, R., Ardizzoni, A., Girardis, M., ... & Blasi, E. (2018). Real-time monitoring of Pseudomonas aeruginosa biofilm formation on endotracheal tubes in vitro. BMC microbiology, 18(1), 1-10.

16. Hoffman, L. R., D'Argenio, D. A., MacCoss, M. J., Zhang, Z., Jones, R. A., & Miller, S. I. (2005). Aminoglycoside antibiotics induce bacterial biofilm formation. Nature, 436(7054), 1171-1175.

17. Palmer, K. L., Aye, L. M., & Whiteley, M. (2007). Nutritional cues control Pseudomonas aeruginosa multicellular behavior in cystic fibrosis sputum. *Journal of bacteriology*, 189(22), 8079-8087.

18. Jørgensen, K. M., Wassermann, T., Johansen, H. K., Christiansen, L. E., Molin, S., Høiby, N., & Ciofu, O. (2015). Diversity of metabolic profiles of cystic fibrosis Pseudomonas aeruginosa during the early stages of lung infection. *Microbiology*, 161(7), 1447-1462.

19. La Rosa, R., Johansen, H. K., & Molin, S. (2019). Adapting to the airways: metabolic requirements of Pseudomonas aeruginosa during the infection of cystic fibrosis patients. *Metabolites*, 9(10), 234.

20. Fox, P. F., & Kelly, A. L. (2006). Indigenous enzymes in milk: Overview and historical aspects—Part 1. *International Dairy Journal*, 16(6), 500-516.

21. Kesel, S., von Bronk, B., García, C. F., Götz, A., Lieleg, O., & Opitz, M. (2017). Matrix composition determines the dimensions of Bacillus subtilis NCIB 3610 biofilm colonies grown on LB agar. RSC advances, 7(51), 31886-31898.

22. Suarez, C., Piculell, M., Modin, O., Langenheder, S., Persson, F., & Hermansson, M. (2019). Thickness determines microbial community structure and function in nitrifying biofilms via deterministic assembly. *Scientific reports*, 9(1), 1-10.

23. Why are biofilm chemistry and biology so spatially heterogeneous? Gradients and a interactive model. (2019, June 12). https://www.cs.montana.edu/webworks/projects/biofilmbook/contents/chapters/chapter006/section003/blue/page001.html.

24. Glud, R. N., Ramsing, N. B., & Revsbech, N. P. (1992). PHOTOSYNTHESIS AND PHOTOSYNTHESIS-COUPLED RESPIRATION IN NATURAL BIOFILMS QUANTIFIED WITH OXYGEN MICROSENSORS 1. *Journal of Phycology*, 28(1), 51-60.

25. Fagerlind, M. G., Webb, J. S., Barraud, N., McDougald, D., Jansson, A., Nilsson, P., ... & Rice, S. A. (2012). Dynamic modelling of cell death during biofilm development. *Journal of theoretical biology*, 295, 23-36.

26. Picioreanu, C., van Loosdrecht, M., & Heijnen, J. (1999). Multidimensional modeling of biofilm structure. Delft University of Technology, Faculty of Applied Sciences.

27. Gomez, J. A., Höffner, K., & Barton, P. I. (2014). DFBAlab: a fast and reliable MATLAB code for dynamic flux balance analysis. *BMC bioinformatics*, 15(1), 1-10.

28. Process Systems Engineering Laboratory. Welcome to the Process Systems Engineering Laboratory | Process Systems Engineering Laboratory. (2021, April 22). https://yoric.mit.edu/welcome-process-systems-engineering-laboratory#gsc.tab=0.

29. Du, B., Zielinski, D. C., Kavvas, E. S., Dräger, A., Tan, J., Zhang, Z., ... & Palsson, B. O. (2016). Evaluation of rate law approximations in bottom-up kinetic models of metabolism. *BMC systems biology*, 10(1), 1-15.

30. Kim, O. D., Rocha, M., & Maia, P. (2018). A review of dynamic modeling approaches and their application in computational strain optimization for metabolic engineering. *Frontiers in microbiology*, 9, 1690.

31. Oberhardt, M. A., Puchałka, J., Fryer, K. E., Martins dos Santos, V. A., & Papin, J. A. (2008). Genome-scale metabolic network analysis of the opportunistic pathogen Pseudomonas aeruginosa PAO1.

32. M. Henson, Interviewee, "Masters Research Meetings.". [Interview].

33. Kantor, I., Robineau, J. L., Butun, H., & Marechal, F. (2020). A mixed-integer linear programming formulation for optimizing multi-scale material and energy integration. *Frontiers in Energy Research*, 8(ARTICLE), 49.

34. Vanderbei, R. J. (2015). Linear programming (Vol. 3). Heidelberg: Springer.

35. Elert, G. (2021, June 12). Mass of a Bacterium. Mass of a Bacterium - The Physics Factbook. https://hypertextbook.com/facts/2003/LouisSiu.shtml#:~:text=A%20typical%20mass%20of%20a,a%20wide%20range%20of%20environments.

36. Klipp, E., Herwig, R., Kowald, A., Wierling, C., & Lehrach, H. (2005). Systems biology in practice: concepts, implementation and application. John Wiley & Sons.

37. Henson, M. A. (2015). Genome-scale modelling of microbial metabolism with temporal and spatial resolution. *Biochemical Society Transactions*, 43(6), 1164-1171.

38. Phalak, P., Chen, J., Carlson, R. P., & Henson, M. A. (2016). Metabolic modeling of a chronic wound biofilm consortium predicts spatial partitioning of bacterial species. *BMC systems biology*, 10(1), 1-20.

39. Henson, M. A., & Phalak, P. (2017). Byproduct cross feeding and community stability in an in silico biofilm model of the gut microbiome. *Processes*, 5(1), 13.

40. Henson, M. A., & Phalak, P. (2017). Microbiota dysbiosis in inflammatory bowel diseases: in silico investigation of the oxygen hypothesis. *BMC systems biology*, 11(1), 1-15.

41. Magana, M., Sereti, C., Ioannidis, A., Mitchell, C. A., Ball, A. R., Magiorkinis, E., ... & Tegos, G. P. (2018). Options and limitations in clinical investigation of bacterial biofilms. *Clinical Microbiology Reviews*, 31(3), e00084-16.

42. Ribeiro, A. C., Lobo, V. M., Leaist, D. G., Natividade, J. J., Veríssimo, L. P., Barros, M. C., & Cabral, A. M. (2005). Binary diffusion coefficients for aqueous solutions of lactic acid. *Journal of Solution Chemistry*, 34(9), 1009-1016.

43. Phalak, P., & Henson, M. A. (2019). Metabolic modelling of chronic wound microbiota predicts mutualistic interactions that drive community composition. *Journal of applied microbiology*, *127*(5), 1576-1593.

44. Eschbach, M., Schreiber, K., Trunk, K., Buer, J., Jahn, D., & Schobert, M. (2004). Long-term anaerobic survival of the opportunistic pathogen Pseudomonas aeruginosa via pyruvate fermentation. *Journal of bacteriology*, 186(14), 4596-4604.

45. Schobert, M., & Jahn, D. (2010). Anaerobic physiology of Pseudomonas aeruginosa in the cystic fibrosis lung. *International Journal of Medical Microbiology*, 300(8), 549-556.

46. Arai, H. (2011). Regulation and function of versatile aerobic and anaerobic respiratory metabolism in Pseudomonas aeruginosa. *Frontiers in microbiology*, 2, 103.

47. La Rosa, R., Johansen, H. K., & Molin, S. (2018). Convergent metabolic specialization through distinct evolutionary paths in Pseudomonas aeruginosa. MBio, 9(2), e00269-18.

48. Mathee, K., Narasimhan, G., Valdes, C., Qiu, X., Matewish, J. M., Koehrsen, M., ... & Lory, S. (2008). Dynamics of Pseudomonas aeruginosa genome evolution. *Proceedings of the National Academy of Sciences*, 105(8), 3100-3105.

49. Hogardt, M., & Heesemann, J. (2010). Adaptation of Pseudomonas aeruginosa during persistence in the cystic fibrosis lung. *International Journal of Medical Microbiology*, 300(8), 557-562.

50. Lin, Y. C., Cornell, W. C., Jo, J., Price-Whelan, A., & Dietrich, L. E. (2018). The Pseudomonas aeruginosa complement of lactate dehydrogenases enables use of d-and l-lactate and metabolic cross-feeding. *MBio*, 9(5), e00961-18.

51. Kalkowski, I., & Conrad, R. (1991). Metabolism of nitric oxide in denitrifying Pseudomonas aeruginosa and nitrate-respiring Bacillus cereus. *FEMS microbiology letters*, 82(1), 107-111.

52. Hernandez, D., Dias, F. M., & Rowe, J. J. (1991). Nitrate transport and its regulation by O2 in Pseudomonas aeruginosa. *Archives of biochemistry and biophysics*, 286(1), 159-163.